Qualitative dynamics, for cyclists

11

I.1. Introduction to conjugacy problems for diffeomorphisms. This is a survey article on the area of global analysis defined by differentiable dynamical systems or equivalently the action (differentiable) of a Lie group G on a manifold M. Here Diff(M) is the group of all diffeomorphisms of M and a diffeomorphism is a differentiable map with a differentiable inverse. (. . .) Our problem is to study the global structure, i.e., all of the orbits of M.

Stephen Smale, *Differentiable Dynamical Systems*

In Sections **??** and 10.1 we introduced the concept of partitioning the state space, in any way you please. In Chapter 5 we established that stability eigenvalues of periodic orbits are invariants of a given flow. The invariance of stabilities of a periodic orbit is a local property of the flow.

For the Rössler flow of Example 3.3, we have learned that the attractor is very thin, but otherwise the return maps that we found were disquieting – Fig. 3.3 did not appear to be a one-to-one map. This apparent loss of invertibility is an artifact of projection of higher-dimensional return maps onto lower-dimensional subspaces. As the choice of lower-dimensional subspace is arbitrary, the resulting snapshots of return maps look rather arbitrary, too. Other projections might look even less suggestive.

Such observations beg a question: Does there exist a "natural", intrinsically optimal coordinate system in which we should plot of a return map?

As we shall now argue (see also Section 12.1), the answer is yes: The intrinsic coordinates are given by the stable / unstable manifolds, and a return map should be plotted as a map from the unstable manifold back onto the immediate neighborhood of the unstable manifold.

In this chapter we show that every equilibrium point and every periodic orbit carries with it stable and unstable manifolds which provide a topologically invariant *global* foliation of the state space. This qualitative dynamics of stretching and mixing enables us to partition the state space and assign symbolic dynamics itineraries to trajectories.

Given an itinerary, the topology of stretching and folding fixes the relative spatial ordering of trajectories, and separates the admissible

and inadmissible itineraries. The level is distinctly cyclist, in distinction to the pedestrian tempo of the preceding chapter. Skip this chapter unless you really need to get into nitty-gritty details of symbolic dynamics.

fast track
Chapter 13, p. 173

11.1 Recoding, symmetries, tilings

In Chapter 9 we made a claim that if there is a symmetry of dynamics, we must use it. So let's take the old pinball game and "quotient the state space by the symmetry or "desymmetrize."

Though a useful tool, Markov partitioning is not without drawbacks. One glaring shortcoming is that Markov partitions are not unique: any of many different partitions might do the job. The 3-disk system offers a simple illustration of different Markov partitioning strategies for the same dynamical system.

The $\mathcal{A} = \{1, 2, 3\}$ symbolic dynamics for 3-disk system is neither unique, nor necessarily the smartest one - before proceeding it pays to exploit the symmetries of the pinball in order to obtain a more efficient description. In Chapter **??** we shall be handsomely rewarded for our labors.

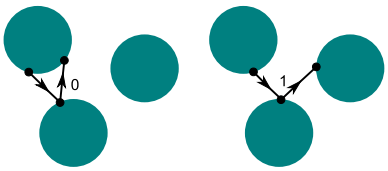

Fig. 11.1 Binary labeling of trajectories of the symmetric 3-disk pinball; a bounce in which the trajectory returns to the preceding disk is labeled 0, and a bounce which results in continuation to the third disk is labeled 1.

10.1, page 133
9.1, page 115
10.2, page 133

As the three disks are equidistantly spaced, our game of pinball has a sixfold symmetry. For instance, the cycles $\overline{12}$, $\overline{23}$, and $\overline{13}$ are related to each other by rotation by $\pm 2\pi/3$ or, equivalently, by a relabeling of the disks. The disk labels are arbitrary; what is important is how a trajectory evolves as it hits subsequent disks, not what label the starting disk had. We exploit this symmetry by *recoding*, in this case replacing the absolute disk labels by relative symbols, indicating the type of the collision. For the 3-disk game of pinball there are two topologically distinct kinds of collisions, Fig. 11.1:

$$s_i = \begin{cases} 0 & : \quad \text{pinball returns to the disk it came from} \\ 1 & : \quad \text{pinball continues to the third disk} . \end{cases} \tag{11.1}$$

This *binary* symbolic dynamics has two immediate advantages over the ternary one; the prohibition of self-bounces is automatic, and the coding utilizes the symmetry of the 3-disk pinball game in elegant manner. If the disks are sufficiently far apart there are no further restrictions on symbols, the symbolic dynamics is complete, and *all* binary sequences (see Table 10.1) are admissible itineraries.

Example 11.1 Recoding ternary symbolic dynamics in binary:
Given a ternary sequence and labels of 2 preceding disks, rule (11.1) fixes the subsequent binary symbols. Here we list an arbitrary ternary itinerary, and the corresponding binary sequence:

$$\begin{array}{rcl} \text{ternary} & : & 3\ 1\ 2\ 1\ 3\ 1\ 2\ 3\ 2\ 1\ 2\ 3\ 1\ 3\ 2\ 3 \\ \text{binary} & : & \cdot\ 1\ 0\ 1\ 0\ 1\ 1\ 0\ 1\ 0\ 1\ 1\ 0\ 1\ 0 \end{array} \tag{11.2}$$

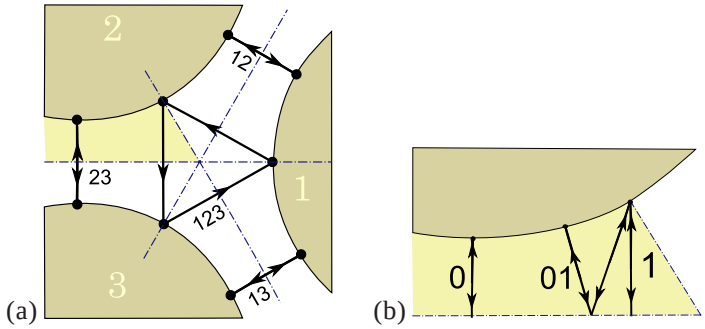

Fig. 11.2 The 3-disk game of pinball with the disk radius : center separation ratio a:R = 1:2.5. (a) 2-cycles $\overline{12}$, $\overline{13}$, $\overline{23}$, and 3-cycles $\overline{123}$ and $\overline{132}$ (not drawn). (b) The fundamental domain, i.e., the small 1/6th wedge indicated in (a), consisting of a section of a disk, two segments of symmetry axes acting as straight mirror walls, and an escape gap. The above five cycles restricted to the fundamental domain are the two fixed points $\overline{0}$, $\overline{1}$. See Fig. 9.2 for cycle $\overline{10}$ and further examples.

The first 2 disks initialize the trajectory and its direction; $3 \mapsto 1 \mapsto 2 \mapsto \cdots$. Due to the 3-disk symmetry the six distinct 3-disk sequences initialized by 12, 13, 21, 23, 31, 32 respectively have the same weights, the same size partitions, and are coded by a single binary sequence. For periodic orbits, the equivalent ternary cycles reduce to binary cycles of 1/3, 1/2 or the same length. How this works is best understood by inspection of Table 11.1, Fig. 11.1 and Fig. 9.5.

The 3-disk game of pinball is tiled by six copies of the *fundamental domain*, a one-sixth slice of the full 3-disk system, with the symmetry axes acting as reflecting mirrors, see Fig. 11.1 (b). Every global 3-disk trajectory has a corresponding fundamental domain mirror trajectory obtained by replacing every crossing of a symmetry axis by a reflection. Depending on the symmetry of the full state space trajectory, a repeating binary symbols block corresponds either to the full periodic orbit or to a relative periodic orbit (examples are shown in Fig. 11.1 and Table 11.1). An irreducible segment corresponds to a periodic orbit in the fundamental domain. Table 11.1 lists some of the shortest binary periodic orbits, together with the corresponding full 3-disk symbol sequences and orbit symmetries. For a number of deep reasons that will be elucidated in Chapter **??**, life is much simpler in the fundamental domain than in the full system, so whenever possible our computations will be carried out in the fundamental domain.

9.2, page 115

Example 11.2 C_2 **recoded:**

As the simplest example of implementing the above scheme consider the C_2 symmetry of Example 9.3. For our purposes, all that we need to know here is that each orbit or configuration is uniquely labeled by an infinite string $\{s_i\}$, $s_i = +, -$ and that the dynamics is invariant under the $+ \leftrightarrow -$ interchange, i.e., it is C_2 symmetric. The C_2 symmetry cycles separate into two classes, the self-dual configurations $+-$, $++--$, $+++---$, $+--+-++-$, $\cdots$, with

$\tilde{p}$	p	$\mathbf{g}_{\tilde{p}}$
0	1 2	σ_{12}
1	1 2 3	C_3
01	12 13	σ_{23}
001	121 232 313	C_3
011	121 323	σ_{13}
0001	1212 1313	σ_{23}
0011	1212 3131 2323	C_3^2
0111	1213 2123	σ_{12}
00001	12121 23232 31313	C_3
00011	12121 32323	σ_{13}
00101	12123 21213	σ_{12}
00111	12123	e
01011	12131 23212 31323	C_3
01111	12132 13123	σ_{23}
000001	121212 131313	σ_{23}
000011	121212 313131 232323	C_3^2
000101	121213	e
000111	121213 212123	σ_{12}
001011	121232 131323	σ_{23}
001101	121231 323213	σ_{13}
001111	121231 232312 313123	C_3
010111	121312 313231 232123	C_3^2
011111	121321 323123	σ_{13}
0000001	1212121 2323232 3131313	C_3
0000011	1212121 3232323	σ_{13}
0000101	1212123 2121213	σ_{12}
0000111	1212123	e
...	...	...

Table 11.1 C_{3v} correspondence between the binary labeled fundamental domain prime cycles $\tilde{p}$ and the full 3-disk ternary labeled cycles p, together with the C_{3v} transformation that maps the end point of the $\tilde{p}$ cycle into the irreducible segment of the p cycle, see Section 9.2. Breaks in the above ternary sequences mark repeats of the irreducible segment. The multiplicity of p cycle is $m_p = 6n_{\tilde{p}}/n_p$. The shortest pair of the fundamental domain cycles related by time reversal (but no spatial symmetry) are the 6-cycles $\overline{001011}$ and $\overline{001101}$.

$\tilde{p}$	p	m_p
1	$+$	2
0	$-+$	1
01	$--\ ++$	1
001	$-++$	2
011	$---\ +++$	1
0001	$-+--\ +-++$	1
0011	$-+++$	2
0111	$----\ ++++$	1
00001	$-+-+-$	2
00011	$-+---\ +-++$	1
00101	$-+-+-\ +--++$	1
00111	$-+---\ +-++$	1
01011	$--+++$	2
01111	$-----\ ++++$	1
001011	$-++---\ +--+++$	1
001101	$-+++--\ +---++$	1

Table 11.2 Correspondence between the C_2 symmetry reduced cycles $\tilde{p}$ and the standard Ising model periodic configurations p, together with their multiplicities m_p. Also listed are the two shortest cycles (length 6) related by time reversal, but distinct under C_2.

multiplicity $m_p = 1$, and the asymmetric pairs $+, -, ++-, --+, \cdots$, with multiplicity $m_p = 2$. For example, as there is no absolute distinction between the "up" and the "down" spins, or the "left" or the "right" lobe, $\Lambda_+ = \Lambda_-$, $\Lambda_{++-} = \Lambda_{+--}$, and so on.

The symmetry reduced labeling $\rho_i \in \{0, 1\}$ is related to the standard $s_i \in \{+, -\}$ Ising spin labeling by

??, page ??

$$\begin{aligned} &\text{If} \quad s_i = s_{i-1} \quad \text{then} \quad \rho_i = 1 \\ &\text{If} \quad s_i \neq s_{i-1} \quad \text{then} \quad \rho_i = 0 \end{aligned} \tag{11.3}$$

For example, $\overline{+} = \cdots +++\cdots$ maps into $\cdots 111 \cdots = \overline{1}$ (and so does $\overline{-}$), $\overline{-+} = \cdots -+-+\cdots$ maps into $\cdots 000 \cdots = \overline{0}$, $\overline{-++-} = \cdots --++--++\cdots$ maps into $\cdots 0101 \cdots = \overline{01}$, and so forth. A list of such reductions is given in Table 11.2.

Example 11.3 C_{3v} recoded - 3-disk game of pinball:

The C_{3v} recoding can be worked out by a glance at Fig. 11.1 (a) (continuation of Example 9.4). For the symmetric 3-disk game of pinball the fundamental domain is bounded by a disk segment and the two adjacent sections of

the symmetry axes that act as mirrors (see Fig. 11.1 (b)). The three symmetry axes divide the space into six copies of the fundamental domain. Any trajectory on the full space can be pieced together from bounces in the fundamental domain, with symmetry axes replaced by flat mirror reflections. The binary $\{0,1\}$ reduction of the ternary three disk $\{1,2,3\}$ labels has a simple geometric interpretation: a collision of type 0 reflects the projectile to the disk it comes from (back–scatter), whereas after a collision of type 1 projectile continues to the third disk. For example, $\overline{23} = \cdots 232323 \cdots$ maps into $\cdots 000 \cdots = \overline{0}$ (and so do $\overline{12}$ and $\overline{13}$), $\overline{123} = \cdots 12312 \cdots$ maps into $\cdots 111 \cdots = \overline{1}$ (and so does $\overline{132}$), and so forth. A list of such reductions for short cycles is given in Table 11.1, Fig. 11.1 and Fig. 9.5.

11.2 Going global: Stable/unstable manifolds

A neighborhood of a trajectory deforms as it is transported by the flow. In the linear approximation, the stability matrix A describes this shearing of an infinitesimal neighborhood in an infinitesimal time step. The shearing after finite time is described by the fundamental matrix M^t. Its eigenvalues and eigendirections describe deformation of an initial infinitesimal sphere of neighboring trajectories into an ellipsoid time t later. Nearby trajectories separate exponentially along the unstable directions, approach each other along the stable directions, and maintain their distance along the marginal directions.

The fixed or periodic point x^* fundamental matrix $M_p(x^*)$ eigenvectors (5.9) form a rectilinear coordinate frame in which the flow into, out of, or encircling the fixed point is linear in the sense of Section 4.2. These eigendirections are numerically continued into global curvilinear invariant manifolds as follows.

The global continuations of the local stable, unstable eigendirections are called the *stable*, respectively *unstable manifolds*. They consist of all points which march into the fixed point forward, respectively backward in time

$$\begin{aligned} W^s &= \left\{x \in \mathcal{M} : f^t(x) - x^* \to 0 \text{ as } t \to \infty\right\} \\ W^u &= \left\{x \in \mathcal{M} : f^{-t}(x) - x^* \to 0 \text{ as } t \to \infty\right\} . \end{aligned} \tag{11.4}$$

The stable / unstable manifolds of a flow are rather hard to visualize, so as long as we are not worried about a global property such as the number of times they wind around a periodic trajectory before completing a par-course, we might just as well look at their Poincaré section return maps. Stable, unstable manifolds for maps are defined by

$$\begin{aligned} W^s &= \left\{x \in \mathcal{P} : f^n(x) - x^* \to 0 \text{ as } n \to \infty\right\} \\ W^u &= \left\{x \in \mathcal{P} : f^{-n}(x) - x^* \to 0 \text{ as } n \to \infty\right\} . \end{aligned} \tag{11.5}$$

Eigenvectors (real or complex pairs) of fundamental matrix $M_p(x^*)$ play a special role - on them the action of the dynamics is the linear multiplication by Λ_i (for a real eigenvector) along 1-d invariant curve $W^{u,s}_{(i)}$ or spiral in / out action in a 2-D surface (for a complex pair). For $n \to \infty$

a finite segment on $W^s_{(e)}$, respectively $W^u_{(c)}$ converges to the linearized map eigenvector $\mathbf{e}^{(e)}$, respectively $\mathbf{e}^{(c)}$. In this sense each eigenvector defines a (curvilinear) axis of the stable, respectively unstable manifold.

Conversely, we can use an arbitrarily small segment of a fixed point eigenvector to construct a finite segment of the associated manifold. Precise construction depends on the type of the eigenvalue(s).

Expanding real and positive eigendirection. Consider ith expanding eigenvalue, eigenvector pair $(\Lambda_i, \mathbf{e}_i)$ computed from J evaluated at a cycle point,

$$J(x)\mathbf{e}_i(x) = \Lambda_i \mathbf{e}_i(x)\,, \quad x \in p\,, \quad \Lambda_i > 1\,. \tag{11.6}$$

Take an infinitesimal eigenvector $\epsilon\,\mathbf{e}_i(x)$, $\epsilon \ll 1$, and its image $J_p(x)\epsilon\,\mathbf{e}_i(x) = \Lambda_i \epsilon\,\mathbf{e}_i(x)$. Sprinkle the interval $|\Lambda_i - 1|\epsilon$ with a large number of points x_m, equidistantly spaced on logarithmic scale $\ln|\Lambda_i - 1| + \ln\epsilon$. The successive images of these points $f(x_j)$, $f^2(x_j)$, $\cdots$, $f^m(x_j)$ trace out the curvilinear unstable manifold in direction $\mathbf{e}_i$. Repeat for $-\epsilon\,\mathbf{e}_i(x)$.

Contracting real, positive eigendirection. Reverse the action of the map backwards in time. This turns a contracting direction into an expanding one, tracing out the curvilinear stable manifold in continuation of $\epsilon\,\mathbf{e}_j$.

Expanding/contracting real negative eigendirection. As above, but every even iterate $f^2(x_j)$, $f^4(x_j)$, $f^6(x_j)$ continues in the direction $\mathbf{e}_i$, every odd one in the direction $-\mathbf{e}_i$.

Complex eigenvalue pair. Construct an orthonormal pair of eigenvectors spanning the plane $\{\epsilon\,\mathbf{e}_j, \epsilon\,\mathbf{e}_{j+1}\}$. Iteration of the annulus between an infinitesimal circle and its image by J spans the spiralling / circle unstable manifold of the complex eigenvalue pair $\{\Lambda_i, \Lambda_{i+1} = \Lambda_i^*\}$.

11.3 Horseshoes

If a flow is locally unstable but globally bounded, any open ball of initial points will be stretched out and then folded back. An example is a 3-dimensional invertible flow sketched in Fig. 10.2 which returns an area of a Poincaré section of the flow stretched and folded into a "horseshoe", such that the initial area is intersected at most twice. Run backwards, the flow generates the backward horseshoe which intersects the forward horseshoe at most 4 times, and so forth. Such flows exist, and are easily constructed - an example is the Rössler system , discussed in Example 3.3.

11.1, page 152

Now we shall construct an example of a locally unstable but globally bounded mapping which returns an initial area stretched and folded into a "horseshoe", such that the initial area is intersected at most twice. We shall refer to such mappings with at most 2^n transverse self-intersections at the nth iteration as the *once-folding* maps.

As an example is afforded by the 2-dimensional *Hénon map*

3.5, page 50

$$\begin{aligned} x_{n+1} &= 1 - ax_n^2 + by_n \\ y_{n+1} &= x_n\,. \end{aligned} \tag{11.7}$$

The Hénon map models qualitatively the Poincaré section return map of Fig. 10.2. For $b = 0$ the Hénon map reduces to the parabola (10.7), and, as shown in Sections 3.3 and **??**, for $b \neq 0$ it is kind of a fattened parabola; by construction, it takes a rectangular initial area and returns it bent as a horseshoe.

For definitiveness, fix the parameter values to $a = 6$, $b = 0.9$. The map is quadratic, so it has 2 fixed points $x_0 = f(x_0)$, $x_1 = f(x_1)$ indicated in Fig. 11.3 (a). For the parameter values at hand, they are both unstable. If you start with a small ball of initial points centered around x_1, and iterate the map, the ball will be stretched and squashed along the line W_1^u. Similarly, a small ball of initial points centered around the other fixed point x_0 iterated backward in time,

$$\begin{aligned} x_{n-1} &= y_n \\ y_{n-1} &= -\frac{1}{b}(1 - a y_n^2 - x_n)\,, \end{aligned} \tag{11.8}$$

traces out the line W_0^s. W_0^s is the stable manifold of x_0 fixed point, and W_1^u is the unstable manifold of x_1 fixed point, defined in Section 11.2. Their intersections enclose the crosshatched region $\mathcal{M}_{\cdot}$. Any point outside W_1^u border of $\mathcal{M}_{\cdot}$ escapes to infinity forward in time, while any point outside W_0^s border escapes to infinity backwards in time. In this way the unstable - stable manifolds define topologically, invariant and optimal $\mathcal{M}_{\cdot}$ initial region; all orbits that stay confined for all times are confined to $\mathcal{M}_{\cdot}$.

Iterated one step forward, the region $\mathcal{M}_{\cdot}$ is stretched and folded into a *smale* horseshoe drawn in Fig. 11.3 (b). The horseshoe fattened parabola shape is the consequence of the quadratic form x^2 in (11.7). Parameter a controls the amount of stretching, while the parameter b controls the amount of compression of the folded horseshoe. The case $a = 6$, $b = 0.9$ considered here corresponds to strong stretching and weak compression. Label the two forward intersections $f(\mathcal{M}_{\cdot}) \cap \mathcal{M}_{\cdot}$ by $\mathcal{M}_{s\cdot}$, with $s \in \{0, 1\}$, Fig. 11.3 (b). The horseshoe consists of the two strips $\mathcal{M}_{0\cdot}, \mathcal{M}_{1\cdot}$, and the bent segment that lies entirely outside the W_1^u line. As all points in this segment escape to infinity under forward iteration, this region can safely be cut out and thrown away.

Iterated one step backwards, the region $\mathcal{M}_{\cdot}$ is again stretched and folded into a horseshoe, Fig. 11.3 (c). As stability and instability are interchanged under time reversal, this horseshoe is transverse to the forward one. Again the points in the horseshoe bend wonder off to infinity as $n \to -\infty$, and we are left with the two (backward) strips $\mathcal{M}_{\cdot 0}, \mathcal{M}_{\cdot 1}$. Iterating two steps forward we obtain the four strips $\mathcal{M}_{11\cdot}, \mathcal{M}_{01\cdot}, \mathcal{M}_{00\cdot}, \mathcal{M}_{10\cdot}$, and iterating backwards we obtain the four strips $\mathcal{M}_{\cdot 00}, \mathcal{M}_{\cdot 01}, \mathcal{M}_{\cdot 11}, \mathcal{M}_{\cdot 10}$ transverse to the forward ones just as for 3-disk pinball game Fig. 10.9. Iterating three steps forward we get an 8 strips, and so on *ad infinitum*.

What is the significance of the subscript $_{\cdot 011}$ which labels the $\mathcal{M}_{\cdot 011}$ backward strip? The two strips $\mathcal{M}_{\cdot 0}, \mathcal{M}_{\cdot 1}$ partition the state space into two regions labeled by the two-letter alphabet $\mathcal{A} = \{0, 1\}$. $S^+ = .011$ is the *future itinerary* for all $x \in \mathcal{M}_{\cdot 011}$. Likewise, for the forward strips

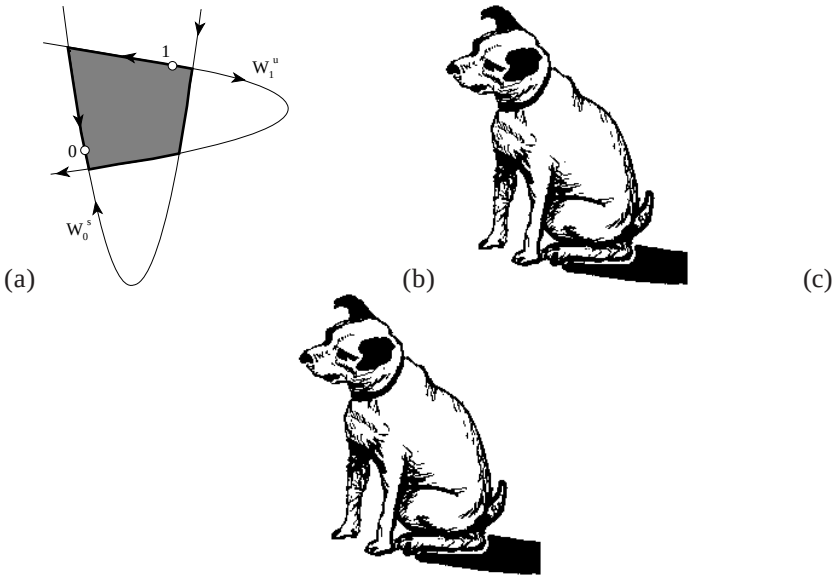

Fig. 11.3 The Hénon map for $a = 6$, $b = .9$. (a) The fixed points $\overline{0}$, $\overline{1}$, and the segments of the W_0^s stable manifold, W_1^u unstable manifold that enclose the initial (crosshatched) region $\mathcal{M}_{.}$. (b) The forward horseshoe $f(\mathcal{M}_{.})$. (c) The backward horseshoe $f^{-1}(\mathcal{M}_{.})$. Iteration yields a complete Smale horseshoe, with every forward fold intersecting every backward fold.

all $x \in \mathcal{M}_{s_{-m}\cdots s_{-1}s_0.}$ have the *past itinerary* $S^{\text{-}} = s_{-m}\cdots s_{-1}s_0$. Which partition we use to present pictorially the regions that do not escape in m iterations is a matter of taste, as the backward strips are the preimages of the forward ones

$$\mathcal{M}_{0.} = f(\mathcal{M}_{.0})\,, \qquad \mathcal{M}_{1.} = f(\mathcal{M}_{.1})\,.$$

Ω, the non-wandering set (2.2) of $\mathcal{M}_{.}$, is the union of all points whose forward and backward trajectories remain trapped for all time. given by the intersections of all images and preimages of $\mathcal{M}$:

$$\Omega = \left\{ x : x \in \lim_{m,n\to\infty} f^m(\mathcal{M}_{.}) \bigcap f^{-n}(\mathcal{M}_{.}) \right\}\,. \tag{11.9}$$

Two important properties of the Smale horseshoe are that it has a *complete binary symbolic dynamics* and that it is *structurally stable.*

For a *complete* Smale horseshoe every forward fold $f^n(\mathcal{M})$ intersects transversally every backward fold $f^{-m}(\mathcal{M})$, so a unique bi-infinite binary sequence can be associated to every element of the non-wandering set. A point $x \in \Omega$ is labeled by the intersection of its past and future itineraries $S(x) = \cdots s_{-2}s_{-1}s_0.s_1s_2\cdots$, where $s_n = s$ if $f^n(x) \in \mathcal{M}_{.s}$, $s \in \{0, 1\}$ and $n \in \mathbb{Z}$. For sufficiently separated disks, the 3-disk game of pinball Fig. 10.9, is another example of a complete Smale horseshoe; in this case the "folding" region of the horseshoe is cut out of the pic-

ture by allowing the pinballs that fly between the disks to fall off the table and escape.

The system is said to be *structurally stable* if all intersections of forward and backward iterates of $\mathcal{M}$ remain transverse for sufficiently small perturbations $f \to f + \delta$ of the flow, for example, for slight displacements of the disks, or sufficiently small variations of the Hénon map parameters a, b while structural stability is exceedingly desirable, it is also exceedingly rare. About this, more later.

11.4 Spatial ordering

Consider a system for which you have succeeded in constructing a covering symbolic dynamics, such as a well-separated 3-disk system. Now start moving the disks toward each other. At some critical separation a disk will start blocking families of trajectories traversing the other two disks. The order in which trajectories disappear is determined by their relative ordering in space; the ones closest to the intervening disk will be pruned first. Determining inadmissible itineraries requires that we relate the spatial ordering of trajectories to their time ordered itineraries.

11.8, page 153

So far we have rules that, given a state space partition, generate a *temporally* ordered itinerary for a given trajectory. Our next task is the reverse: given a set of itineraries, what is the *spatial* ordering of corresponding points along the trajectories? In answering this question we will be aided by Smale's visualization of the relation between the topology of a flow and its symbolic dynamics by means of "horseshoes".

11.4.1 Symbol square

For a better visualization of 2-dimensional non-wandering sets, fatten the intersection regions until they completely cover a unit square, as in Fig. 11.4. We shall refer to such a "map" of the topology of a given 'stretch & fold' dynamical system as the *symbol square*. The symbol square is a topologically accurate representation of the non-wandering set and serves as a street map for labeling its pieces. Finite memory of m steps and finite foresight of n steps partitions the symbol square into *rectangles* $[s_{-m+1}\cdots s_0.s_1s_2\cdots s_n]$. In the binary dynamics symbol square the size of such rectangle is $2^{-m}\times 2^{-n}$; it corresponds to a region of the dynamical state space which contains all points that share common n future and m past symbols. This region maps in a nontrivial way in the state space, but in the symbol square its dynamics is exceedingly simple; all of its points are mapped by the decimal point shift (10.18)

11.2, page 152

$$\sigma(\cdots s_{-2}s_{-1}s_0.s_1s_2s_3\cdots) = \cdots s_{-2}s_{-1}s_0s_1.s_2s_3\cdots\,, \tag{11.10}$$

For example, the square $[01.01]$ gets mapped into the rectangle $\sigma[01.01] = [010.1]$.

11.3, page 152

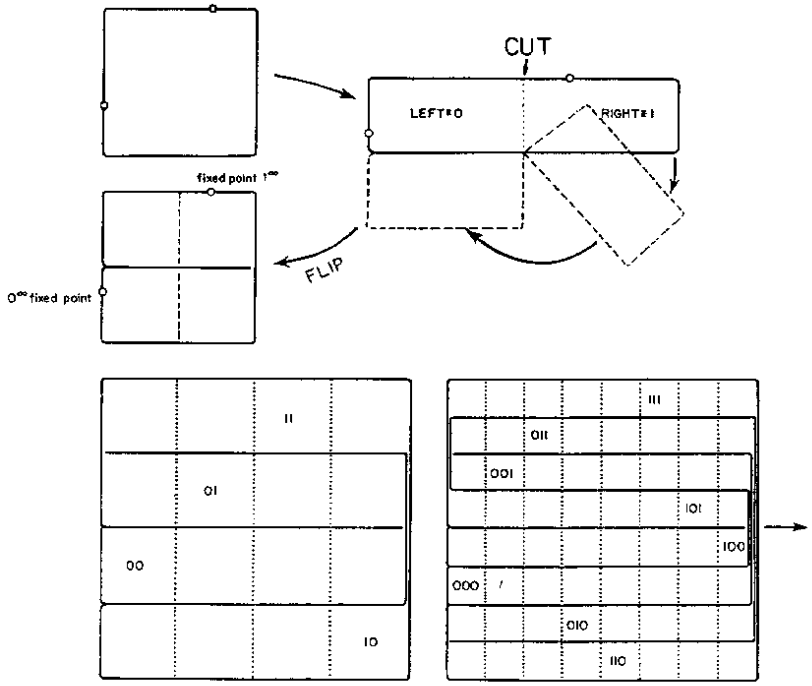

FIG. 4. Iterative construction of the symbol plane.

Fig. 11.4 Kneading Danish Pastry: symbol square representation of an orientation reversing once-folding map obtained by fattening the Smale horseshoe intersections of Fig. 11.3 into a unit square. In the symbol square the dynamics maps rectangles into rectangles by a decimal point shift.

As the horseshoe mapping is a simple repetitive operation, we expect a simple relation between the symbolic dynamics labeling of the horseshoe strips, and their relative placement. The symbol square points $\gamma(S^+)$ with future itinerary S^+ are constructed by converting the sequence of s_n's into a binary number by the algorithm (10.9). This follows by inspection from Fig. 11.4. In order to understand this relation between the topology of horseshoes and their symbolic dynamics, it might be helpful to backtrace to Section 10.2.2 and work through and understand first the symbolic dynamics of one-dimensional unimodal mappings.

11.4, page 153

Under backward iteration the roles of 0 and 1 symbols are interchanged; $\mathcal{M}_0^{-1}$ has the same orientation as $\mathcal{M}$, while $\mathcal{M}_1^{-1}$ has the opposite orientation. We assign to an *orientation preserving* once-folding map the *past topological coordinate* $\delta = \delta(S^-)$ by the algorithm:

11.5, page 153

$$
\begin{aligned}
w_{n-1} &= \begin{cases} w_n & \text{if } s_n = 0 \\ 1 - w_n & \text{if } s_n = 1 \end{cases}, \qquad w_0 = s_0 \\
\delta(S^-) &= 0.w_0 w_{-1} w_{-2} \ldots = \sum_{n=1}^{\infty} w_{1-n}/2^n \,. \qquad (11.11)
\end{aligned}
$$

Such formulas are best derived by quiet contemplation of the action of a folding map, in the same way we derived the future topological coordinate (10.9).

The coordinate pair (δ, γ) maps a point (x, y) in the state space Cantor

set of Fig. 11.3 into a point in the symbol square of Fig. 11.4, preserving the topological ordering; (δ, γ) serves as a topologically faithful representation of the non-wandering set of any once-folding map, and aids us in partitioning the set and ordering the partitions for any flow of this type.

11.5 Pruning

> The complexity of this figure will be striking, and I shall not even try to draw it.
>
> H. Poincaré, on his discovery of homoclinic tangles, *Les méthodes nouvelles de la méchanique céleste*

In general, not all possible itineraries are realized as physical trajectories. Trying to get from "here" to "there" we might find that a short path is excluded by some obstacle, such as a disk that blocks the path, or a potential ridge. To count correctly, we need to $prune$ the inadmissible trajectories, i.e., specify the grammar of the admissible itineraries.

While the complete Smale horseshoe dynamics discussed so far is rather straightforward, we had to get through it in order to be able to approach a situation that resembles more the real life: adjust the parameters of a once-folding map so that the intersection of the backward and forward folds is still transverse, but no longer complete, as in Fig. 13.3.1 (a). The utility of the symbol square lies in the fact that the surviving, admissible itineraries still maintain the same relative spatial ordering as for the complete case.

In the example of Fig. 13.3.1 (a) the rectangles $[10.1]$, $[11.1]$ have been pruned, and consequently *any* trajectory containing blocks $b_1 = 101$, $b_2 = 111$ is pruned. We refer to the border of this primary pruned region as the *pruning front*; another example of a pruning front is drawn in Fig. 13.3.1 (d). We call it a "front" as it can be visualized as a border between admissible and inadmissible; any trajectory whose periodic point would fall to the right of the front in Fig. 13.3.1 is inadmissible, i.e., pruned. The pruning front is a complete description of the symbolic dynamics of once-folding maps. For now we need this only as a concrete illustration of how pruning rules arise.

In the example at hand there are total of two forbidden blocks 101, 111, so the symbol dynamics is a subshift of finite type (10.22). For now we concentrate on this kind of pruning because it is particularly clean and simple. Unfortunately, for a generic dynamical system a subshift of finite type is the exception rather than the rule. Only some repelling sets (like our game of pinball) and a few purely mathematical constructs (called Anosov flows) are structurally stable - for most systems of interest an infinitesimal perturbation of the flow destroys and / or creates an infinity of trajectories, and specification of the grammar requires determination of pruning blocks of arbitrary length. The repercussions are dramatic and counterintuitive; for example, due to the lack of structural stability the transport coefficients such as the de-

terministic diffusion constant of Section **??** are emphatically *not* smooth functions of the system parameters. This generic lack of structural stability is what makes nonlinear dynamics so hard.

The conceptually simpler finite subshift Smale horseshoes suffice to motivate most of the key concepts that we shall need for time being.

11.5.1 Converting pruning blocks into Markov graphs

The complete binary symbolic dynamics is too simple to be illuminating, so we turn next to the simplest example of pruned symbolic dynamics, the finite subshift obtained by prohibition of repeats of one of the symbols, let us say $\_00\_$. This situation arises, for example, in studies of the circle maps, where this kind of symbolic dynamics describes "golden mean" rotations (we shall return to this example in Chapter **??**). Now the admissible itineraries are enumerated by the pruned binary tree of Fig. 10.9 (a), or the corresponding Markov graph Fig. 10.9 (b). We recognize this as the Markov graph example of Fig. 10.5.

13.7, page 192

13.9, page 193

So we can already see the main ingredients of a general algorithm: (1) Markov graph encodes self-similarities of the tree of all itineraries, and (2) if we have a pruning block of length M, we need to descend M levels before we can start identifying the self-similar sub-trees.

Suppose now that, by hook or crook, you have been so lucky fishing for pruning rules that you now know the grammar (10.21) in terms of a finite set of pruning blocks $\mathcal{G} = \{b_1, b_2, \cdots b_k\}$, of lengths $n_{b_m} \leq M$. Our task is to generate all admissible itineraries. What to do?

A Markov graph algorithm.

(1) Starting with the root of the tree, delineate all branches that correspond to all pruning blocks; implement the pruning by removing the last node in each pruning block.

(2) Label all nodes internal to pruning blocks by the itinerary connecting the root point to the internal node. Why? So far we have pruned forbidden branches by looking n_b steps into future for all pruning blocks. into future for pruning block $b = 10010$. However, the blocks with a right combination of past and future $[1.0110]$, $[10.110]$, $[101.10]$ and $[1011.0]$ are also pruned. In other words, any node whose near past coincides with the beginning of a pruning block is potentially dangerous - a branch further down the tree might get pruned.

(3) Add to each internal node all remaining branches allowed by the alphabet, and label them. Why? Each one of them is the beginning point of an infinite tree, a tree that should be similar to another one originating closer to the root of the whole tree.

(4) Pick one of the free external nodes closest to the root of the entire tree, forget the most distant symbol in its past. Does the truncated itinerary correspond to an internal node? If yes, identify the two nodes. If not, forget the next symbol in the past, repeat. If no such

truncated past corresponds to any internal node, identify with the root of the tree.

This is a little bit abstract, so let's say the free external node in question is $[1010.]$. Three time steps back the past is $[010.]$. That is not dangerous, as no pruning block in this example starts with 0. Now forget the third step in the past: $[10.]$ is dangerous, as that is the start of the pruning block $[10.110]$. Hence the free external node $[1010.]$ should be identified with the internal node $[10.]$.

(5) Repeat until all free nodes have been tied back into the internal nodes.

(6) Clean up: check whether every node can be reached from every other node. Remove the transient nodes, i.e., the nodes to which dynamics never returns.

(7) The result is a Markov diagram. There is no guarantee that this is the smartest, most compact Markov diagram possible for given pruning (if you have a better algorithm, teach us), but walks around it do generate all admissible itineraries, and nothing else.

Heavy pruning.

We complete this training by examples by implementing the pruning of Fig. 13.3.1 (d). The pruning blocks are

$$[100.10], [10.1], [010.01], [011.01], [11.1], [101.10]. \tag{11.12}$$

Blocks 01101, 10110 contain the forbidden block 101, so they are redundant as pruning rules. Draw the *pruning tree* as a section of a binary tree with 0 and 1 branches and label each internal node by the sequence of 0's and 1's connecting it to the root of the tree (Fig. 13.3.1 (a). These nodes are the potentially dangerous nodes - beginnings of blocks that might end up pruned. Add the side branches to those nodes (Fig. 13.3.1 (b). As we continue down such branches we have to check whether the pruning imposes constraints on the sequences so generated: we do this by knocking off the leading bits and checking whether the shortened strings coincide with any of the internal pruning tree nodes: $00 \to 0$; $110 \to 10$; $011 \to 11$; $0101 \to 101$ (pruned); $1000 \to 00 \to 00 \to 0$; $10011 \to 0011 \to 011 \to 11$; $01000 \to 0$.

As in the previous two examples, the trees originating in identified nodes are identical, so the tree is "self-similar". Now connect the side branches to the corresponding nodes, Fig. 13.3.1 (d). Nodes "." and 1 are transient nodes; no sequence returns to them, and as you are interested here only in infinitely recurrent sequences, delete them. The result is the finite Markov graph of Fig. 13.3.1 (d); the admissible bi-infinite symbol sequences are generated as all possible walks along this graph.

Summary

Given a partition $\mathcal{A}$ of the state space $\mathcal{M}$, a dynamical system $(\mathcal{M}, f)$ induces topological dynamics (Σ, σ) on the space Σ of all admissible bi–infinite itineraries. The itinerary describes the time evolution of an orbit, while (for 2-d hyperbolic maps) the symbol square describes the spatial ordering of points along the orbit. The rule that everything to one side of the pruning front is forbidden might (in hindsight) seem obvious, but if you have ever tried to work out symbolic dynamics of some "generic" dynamical system, you should be struck by its simplicity: instead of pruning a Cantor set embedded within some larger Cantor set, the pruning front cleanly cuts out a *compact* region in the symbol square and that is all - there are no additional pruning rules.

The symbol square is a useful tool in transforming topological pruning into pruning rules for inadmissible sequences; those are implemented by constructing transition matrices and / or Markov graphs. These matrices are the simplest examples of evolution operators prerequisite to developing a theory of averaging over chaotic flows.

Importance of symbolic dynamics is often grossly unappreciated; as we shall see in Chapters **??** and **??**, coupled with uniform hyperbolicity, the existence of a finite grammar is the crucial prerequisite for construction of zeta functions with nice analyticity properties.

Further reading

Smale horseshoe. S. Smale understood clearly that the crucial ingredient in the description of a chaotic flow is the topology of its non-wandering set, and he provided us with the simplest visualization of such sets as intersections of Smale horseshoes. In retrospect, much of the material covered here can already be found in Smale's fundamental paper [22], but a physicist who has run into a chaotic time series in his laboratory might not know that he is investigating the action (differentiable) of a Lie group G on a manifold M, and that the Lefschetz trace formula is the way to go. If you find yourself mystified by Smale's article abstract about "the action (differentiable) of a Lie group G on a manifold M", quoted on page 143, rereading Chapter **??** might help; for example, the Liouville operators form a Lie group (of symplectic, or canonical transformations) acting on the manifold (p, q).

Kneading theory. The admissible itineraries are studied in Refs. [15, 14, 16, 17], as well as many others. We follow here the Milnor-Thurston exposition [16]. They study the topological zeta function for piecewise monotone maps of the interval, and show that for the finite subshift case it can be expressed in terms of a finite dimensional *kneading determinant*. As the kneading determinant is essentially the topological zeta function that we introduce in (13.4), we shall not discuss it here. Baladi and Ruelle have reworked this theory in a series of papers [18–20] and in Ref. [21] replaced it by a power series manipulation. The kneading theory is covered here in P. Dahlqvist's Appendix **??**.

Pruning fronts. The notion of a pruning front was introduced in Ref. [22], and developed by K.T. Hansen for a number of dynamical systems in his Ph.D. thesis [7] and a series of papers [29]- [33]. Detailed studies of pruning fronts are carried out in Refs. [23,25,24]; Ref. [**?**] is the most detailed study carried out so far. The rigorous theory of pruning fronts has been developed by Y. Ishii [26, 27] for the Lozi map, and A. de Carvalho [28] in a very general setting.

The unbearable growth of Markov graphs. A construction of finite Markov partitions is described in Refs. [10, 11], as well as in the innumerably many other references.

If two regions in a Markov partition are not disjoint but share a boundary, the boundary trajectories require special treatment in order to avoid overcounting, see Section **??**. If the image of a trial partition region cuts across only a part of another trial region and thus violates the Markov partition condition (10.4), a further refinement of the partition is needed to distinguish distinct trajectories - Fig. 13.3.1 is an example of such refinements.

The finite Markov graph construction sketched above is not necessarily the minimal one; for example, the Markov graph of Fig. 13.3.1 does not generate only the "fundamental" cycles (see Chapter **??**), but shadowed cycles as well, such as t_{00011} in (13.17). For methods of reduction to a minimal graph, consult Refs. [6, 54, 7]. Furthermore, when one implements the time reversed dynamics by the same algorithm, one usually gets a graph of very different topology even though both graphs generate the same admissible sequences, and have the same determinant. The algorithm described here makes some sense for 1-d dynamics, but is unnatural for 2-d maps whose dynamics it treats as one-dimensional. In practice, generic pruning grows longer and longer, and more plentiful pruning rules. For generic flows the refinements might never stop, and almost always we might have to deal with infinite Markov partitions, such as those that will be discussed in Section 13.6. Not only do the Markov graphs get more and more unwieldy, they have the unpleasant property that every time we add a new rule, the graph has to be constructed from scratch, and it might look very different form the previous one, even though it leads to a minute modification of the topological entropy. The most determined effort to construct such graphs may be the one of Ref. [23]. Still, this seems to be the best technology available, unless the reader alerts us to something superior.

Exercises

(11.1) **A Smale horseshoe.** The Hénon map

$$\begin{bmatrix} x' \\ y' \end{bmatrix} = \begin{bmatrix} 1 - ax^2 + y \\ bx \end{bmatrix} \tag{11.13}$$

maps the (x, y) plane into itself - it was constructed by Hénon [2] in order to mimic the Poincaré section of once-folding map induced by a flow like the one sketched in Fig. 10.2. For definitiveness fix the parameters to $a = 6$, $b = -1$.

a) Draw a rectangle in the (x, y) plane such that its nth iterate by the Hénon map intersects the rectangle 2^n times.

b) Construct the inverse of the (11.13).

c) Iterate the rectangle back in the time; how many intersections are there between the n forward and m backward iterates of the rectangle?

d) Use the above information about the intersections to guess the (x, y) coordinates for the two fixed points, a 2-cycle point, and points on the two distinct 3-cycles from Table 10.1. The exact cycle points are computed in Exercise 12.10.

(11.2) **Kneading Danish pastry.** Write down the $(x, y) \to (x, y)$ mapping that implements the baker's map of Fig. 11.4, together with the inverse mapping. Sketch a few rectangles in symbol square and their forward and backward images. (Hint: the mapping is very much like the tent map (10.6)).

(11.3) **Kneading Danish without flipping.** The baker's map of Fig. 11.4 includes a flip - a map of this type is called an orientation reversing once-folding map. Write down the $(x, y) \to (x, y)$ mapping that implements an orientation preserving baker's map (no flip; Jacobian determinant = 1). Sketch and label the first few foldings of the symbol square.

(11.4) **Fix this manuscript.** Check whether the layers of the baker's map of Fig. 11.4 are indeed ordered as the branches of the alternating binary tree of Fig. 10.7. (They might not be - we have not rechecked them). Draw the correct binary trees that order both the future and past itineraries.

For once-folding maps there are four topologically distinct ways of laying out the stretched and folded image of the starting region,

(a) orientation preserving: stretch, fold upward, as in Fig. **??**

(b) orientation preserving: stretch, fold downward, as in Fig. 13.3.1

(c) orientation reversing: stretch, fold upward, flip, as in Fig. **??**

(d) orientation reversing: stretch, fold downward, flip, as in Fig. 11.4,

with the corresponding four distinct binary-labeled symbol squares. For n-fold 'stretch & fold' flows the labeling would be $n$ary. The intersection $\mathcal{M}_0$ for the orientation preserving Smale horseshoe, Fig. **??**a, is oriented the same way as $\mathcal{M}$, while $\mathcal{M}_1$ is oriented opposite to $\mathcal{M}$. Brief contemplation of Fig. 11.4 indicates that the forward iteration strips are ordered relative to each other as the branches of the alternating binary tree in Fig. 10.7.

Check the labeling for all four cases.

(11.5) **Orientation reversing once-folding map.** By adding a reflection around the vertical axis to the horseshoe map g we get the orientation reversing map $\tilde{g}$ shown in Fig. **??**. $\tilde{Q}_0$ and $\tilde{Q}_1$ are oriented as Q_0 and Q_1, so the definition of the future topological coordinate γ is identical to the γ for the orientation preserving horseshoe. The inverse intersections $\tilde{Q}_0^{-1}$ and $\tilde{Q}_1^{-1}$ are oriented so that $\tilde{Q}_0^{-1}$ is opposite to Q, while $\tilde{Q}_1^{-1}$ has the same orientation as Q. Check that the past topological coordinate δ is given by

$$w_{n-1} = \begin{cases} 1-w_n & \text{if } s_n = 0 \\ w_n & \text{if } s_n = 1 \end{cases}, \qquad w_0 = s_0$$

$$\delta(x) = 0.w_0 w_{-1} w_{-2} \ldots = \sum_{n=1}^{\infty} w_{1-n}/2^n \quad (11.14)$$

(11.6) **Infinite symbolic dynamics.** Let σ be a function that returns zero or one for every infinite binary string: $\sigma : \{0,1\}^{\mathbb{N}} \to \{0,1\}$. Its value is represented by $\sigma(\epsilon_1, \epsilon_2, \ldots)$ where the ϵ_i are either 0 or 1. We will now define an operator $\mathcal{T}$ that acts on observables on the space of binary strings. A function a is an observable if it has bounded variation, that is, if

$$\|a\| = \sup_{\{\epsilon_i\}} |a(\epsilon_1, \epsilon_2, \ldots)| < \infty \,.$$

For these functions

$$\mathcal{T}a(\epsilon_1, \epsilon_2, \ldots) = a(0, \epsilon_1, \epsilon_2, \ldots)\sigma(0, \epsilon_1, \epsilon_2, \ldots) + a(1, \epsilon_1, \epsilon_2, \ldots)\sigma(1, \epsilon_1, \epsilon_2, \ldots) \,.$$

(a) (easy) Consider a finite version T_n of the operator $\mathcal{T}$:

$$T_n a(\epsilon_1, \epsilon_2, \ldots, \epsilon_{1,n}) = a(0, \epsilon_1, \epsilon_2, \ldots, \epsilon_{n-1})\sigma(0, \epsilon_1, \epsilon_2, \ldots, \epsilon_{n-1}) + a(1, \epsilon_1, \epsilon_2, \ldots, \epsilon_{n-1})\sigma(1, \epsilon_1, \epsilon_2, \ldots, \epsilon_{n-1}) \,.$$

Show that T_n is a $2^n \times 2^n$ matrix. Show that its trace is bounded by a number independent of n.

(b) (medium) With the operator norm induced by the function norm, show that $\mathcal{T}$ is a bounded operator.

(c) (hard) Show that $\mathcal{T}$ is not trace class. (Hint: check if $\mathcal{T}$ is compact "trace class" is defined in Appendix **??**.)

(11.7) **Time reversability.**** Hamiltonian flows are time reversible. Does that mean that their Markov graphs are symmetric in all node $\to$ node links, their transition matrices are adjacency matrices, symmetric and diagonalizable, and that they have only real eigenvalues?

(11.8) **3-disk pruning** (Not easy) Show that for 3-disk game of pinball the pruning of orbits starts at $R : a = 2.04821419\ldots$.

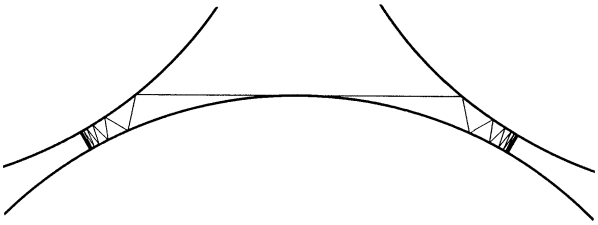

(Kai T. Hansen)

(11.9) **Alphabet {0,1}, prune** $\_1000\_$, $\_00100\_$, $\_01100\_$. This example is motivated by the pruning front description of the symbolic dynamics for the Hénon-type maps.

step 1. $\_1000\_$ prunes all cycles with a $\_000\_$ subsequence with the exception of the fixed point $\overline{0}$; hence we factor out $(1 - t_0)$ explicitly, and prune $\_000\_$ from the rest. This means that x_0 is an isolated fixed point - no cycle stays in its vicinity for more than 2 iterations. In the notation of Section 11.5.1, the alphabet is $\{1, 2, 3;\ \overline{0}\}$, and the remaining pruning rules have to be rewritten in terms of symbols 2=10, 3=100:

step 2. alphabet $\{1, 2, 3;\ \overline{0}\}$, prune $\_33\_$, $\_213\_$,$\_313\_$. This means that the 3-cycle $\overline{3} = \overline{100}$ is pruned and no long cycles stay close enough to it for a single $\_100\_$ repeat. As in example 1?!, prohibition of $\_33\_$ is implemented by dropping the symbol "3" and extending the alphabet by the allowed blocks 13, 23:

step 3. alphabet $\{1,\ 2,\ \underline{13},\ \underline{23};\ \overline{0}\}$, prune $\_2\underline{13}\_$, $\_\underline{23}\,\underline{13}\_$, $\_\underline{13}\,\underline{13}\_$, where $\underline{13} = 13$, $\underline{23} = 23$ are now

used as single letters. Pruning of the repetitions $\underline{13}\,\underline{13}$ (the 4-cycle $\overline{13} = \overline{1100}$ is pruned) yields the **result:** alphabet $\{1, 2, \underline{23}, \underline{113}; \overline{0}\}$, unrestricted 4-ary dynamics. The other remaining possible blocks $\underline{213}$, $\underline{2313}$ are forbidden by the rules of step 3. (continued as Exercise 13.21)

References

[1] E. Hopf, *Ergodentheorie* (Chelsea Publ. Co., New York 1948).

[2] Hopf E 1942 "Abzweigung einer periodischen Lösung," *Bereich. Sächs. Acad. Wiss. Leipzig, Math. Phys. Kl.* **94**, 15 (1942); "Bifurcation of a periodic solution from a stationary solution of a system of differential equations," transl. by L. N. Howard and N. Kopell, in *The Hopf bifurcation and its applications*, J. E. Marsden and M. McCracken, eds., pp. 163-193, (Springer-Verlag, New York 1976).

[3] E. Hopf, "A mathematical example displaying features of turbulence," *Commun. Appl. Math.* **1**, 303 (1948).

[4] T. Bedford, M.S. Keane and C. Series, eds., *Ergodic Theory, Symbolic Dynamics and Hyperbolic Spaces* (Oxford University Press, Oxford, 1991).

[5] M.S. Keane, *Ergodic theory and subshifts of finite type*, in Ref. [4].

[6] B. Kitchens, "Symbolic dynamics, group automorphisms and Markov partition", in *Real and Complex Dynamical Systems*, B. Branner and P. Hjorth, ed. (Kluwer, Dordrecht, 1995).

[7] R. Bowen, *Markov partitions for Axiom A diffeomorphisms"*, *Amer. J. Math.* **92**, 725 (1970).

[8] D. Ruelle, *Transactions of the A.M.S.* **185**, 237 (197?).

[9] R. Bowen, *Periodic orbits for hyperbolic flows*, Amer. J. Math. **94**, 1-30 (1972).

[10] R. Bowen, *Symbolic dynamics for hyperbolic flows*, Amer. J. Math. **95**, 429-460 (1973).

[11] R. Bowen and O.E. Lanford *Math. ??* **??**,

[12] R. Bowen and O.E. Lanford, "*Zeta functions of restrictions"*, pp. 43-49 in *Proceeding of the Global Analysis*, (A.M.S., Providence 1968).

[13] V.M. Alekseev and M.V. Jakobson, *Symbolic dynamics and hyperbolic dynamical systems*, Physics Reports, **75**, 287, (1981).

[14] A. Manning, "Axiom A diffeomorphisms have rational zeta function", *Bull. London Math. Soc.***3**, 215 (1971).

[15] A.N. Sarkovskii, "Coexistence of cycles of a continuous map of a line into itself", *Ukrainian Math. J.* **16**, 61 (1964).

[16] J. Milnor and W. Thurston, *"On iterated maps of the interval"*, in A. Dold and B. Eckmann, eds., *Dynamical Systems, Proceedings, U. of Maryland 1986-87, Lec. Notes in Math.* **1342,** 465 (Springer, Berlin 1988).

[17] W. Thurston, *"On the geometry and dynamics of diffeomorphisms of surfaces"*, *Bull. Amer. Math. Soc.* **19**, 417 (1988).

[18] V. Baladi and D. Ruelle, *"An extension of the theorem of Milnor and Thurston on the zeta functions of interval maps"*, *Ergodic Theory Dynamical Systems* **14**, 621 (1994).

[19] V. Baladi, *"Infinite kneading matrices and weighted zeta functions of interval maps"*, *J. Functional Analysis* **128**, 226 (1995).
[20] D. Ruelle, *"Sharp determinants for smooth interval maps"*, in F. Ledrappier, J. Lewowicz, and S. Newhouse, eds., *Proceedings of Montevideo Conference 1995* (Addison-Wesley, Harlow 1996).
[21] V. Baladi and D. Ruelle, *"Sharp determinants"*, *Invent. Math.* **123**, 553 (1996).
[22] P. Cvitanović, G.H. Gunaratne and I. Procaccia, *Phys. Rev.* **A 38**, 1503 (1988).
[23] G. D'Alessandro, P. Grassberger, S. Isola and A. Politi, "On the topology of the Hénon Map", *J. Phys.* **A 23**, 5285 (1990).
[24] F. Giovannini and A. Politi, "Generating partitions in Hénon-type maps," *Phys. Lett.* **A 161**, 333 (1992);
[25] G. D'Alessandro, S. Isola and A. Politi, "Geometric properties of the pruning front," *Prog. Theor. Phys.* **86**, 1149 (1991).
[26] Y. Ishii, "Towards the kneading theory for Lozi attractors. I. Critical sets and pruning fronts", Kyoto Univ. Math. Dept. preprint (Feb. 1994).
[27] Y. Ishii, "Towards a kneading theory for Lozi mappings. II. A solution of the pruning front conjecture and the first tangency problem", *Nonlinearity* **10**, 731 (1997).
[28] A. de Carvalho, Ph.D. thesis, CUNY New York 1995; "Pruning fronts and the formation of horseshoes", preprint (1997).
[29] K.T. Hansen, *CHAOS* **2**, 71 (1992).
[30] K.T. Hansen, *Nonlinearity* **5**
[31] K.T. Hansen, *Nonlinearity* **5**
[32] K.T. Hansen, *Symbolic dynamics III, The stadium billiard*, to be submitted to *Nonlinearity*
[33] K.T. Hansen, *Symbolic dynamics IV; a unique partition of maps of Hénon type*, in preparation.
[34] Fa-Geng Xie and Bai-Lin Hao, "Counting the number of periods in one-dimensional maps with multiple critical points", *Physica A* **202**, 237 (1994).
[35] M. Benedicks and L. Carleson, *Ann. of Math.*, **122**, 1 (1985).
[36] M. Benedicks and L. Carleson, *IXth Int. Congr. on Mathematical Physics*, B. Simon *et al.*, eds., p.489, (Adam Hilger, Bristol, 1989).
[37] M. Benedicks and L. Carleson, *Ann. of Math.* **133**, 73 (1991).
[38] G. D'Alessandro and A. Politi, "Hierarchical approach to complexity ...", *Phys. Rev. Lett.* **64**, 1609 (1990).
[39] F. Christiansen and A. Politi, "A generating partition for the standard map", *Phys. Rev. E.* **51**, 3811 (1995); `chao-dyn/9411005`
[40] F. Christiansen and A. Politi, "Guidelines for the construction of a generating partition in the standard map", *Physica D* **109**, 32 (1997).
[41] F. Christiansen and A. Politi, "Symbolic encoding in symplectic maps", *Nonlinearity* **9**, 1623 (1996).
[42] F. Christiansen and A. Politi, "Guidelines for the construction of a generating partition in the standard map", *Physica D* **109**, 32 (1997).
[43] T. Hall, "Fat one-dimensional representatives of pseudo-Anosov

isotopy classes with minimal periodic orbit structure", *Nonlinearity* **7**, 367 (1994).
[44] P. Cvitanović and K.T. Hansen, "Symbolic dynamics of the wedge billiard", Niels Bohr Inst. preprint (Nov. 1992)
[45] P. Cvitanović and K.T. Hansen, "Bifurcation structures in maps of Hénon type", *Nonlinearity* **11**, 1233 (1998).
[46] R.W. Easton, "Trellises formed by stable and unstable manifolds in plane", *Trans. Am. Math. Soc.***294**, 2 (1986).
[47] V. Rom-Kedar, "Transport rates of a class of two-dimensional maps and flows", *Physica D* **43**, 229 (1990);
[48] V. Daniels, M. Vallières and J-M. Yuan, "Chaotic scattering on a double well: Periodic orbits, symbolic dynamics, and scaling", *Chaos*, **3**, 475, (1993).
[49] P.H. Richter, H.-J. Scholz and A. Wittek, "A Breathing Chaos", *Nonlinearity* **1**, 45 (1990).
[50] F. Hofbauer, "Periodic points for piecewise monotone transformations", *Ergod. The. and Dynam Sys.* **5**, 237 (1985).
[51] F. Hofbauer, "Piecewise invertible dynamical systems", *Prob. Th. Rel. Fields* **72**, 359 (1986).
[52] K.T. Hansen, "Pruning of orbits in 4-disk and hyperbola billiards", *CHAOS* **2**, 71 (1992).
[53] G. Troll, "A devil's staircase into chaotic scattering", *Pysica D* **50**, 276 (1991)
[54] P. Grassberger, "Toward a quantitative theory of self-generated Complexity", *Int. J. Theor. Phys* **25**, 907 (1986).
[55] D.L. Rod, *J. Diff. Equ.* **14**, 129 (1973).
[56] R.C. Churchill, G. Pecelli and D.L. Rod, *J. Diff. Equ.* **17**, 329 (1975).
[57] R.C. Churchill, G. Pecelli and D.L. Rod, in G. Casati and J. Ford, eds., *Como Conf. Proc. on Stochastic Behavior in Classical and Quantum Hamiltonian Systems* (Springer, Berlin 1976).
[58] R. Mainieri, Ph. D. thesis, New York University (Aug 1990); *Phys. Rev.* **A 45**,3580 (1992)
[59] M.J. Giannoni and D. Ullmo, "Coding chaotic billiards: I. Noncompact billiards on a negative curvature manifold", *Physica* **D 41**, 371 (1990).
[60] D. Ullmo and M.J. Giannoni, "Coding chaotic billiards: II. Compact billiards defined on the psudosphere", *Physica* **D 84**, 329 (1995).
[61] H. Solari, M. Natiello and G.B. Mindlin, "*Nonlinear Physics and its Mathematical Tools*", (IOP Publishing Ltd., Bristol, 1996).
[62] R. Gilmore, "Topological analysis of chaotic dynamical systems", submitted to *Rev. Mod. Phys.* (1997).
[63] P. Dahlqvist, *On the effect of pruning on the singularity structure of zeta functions*, J. Math. Phys. **38**, 4273 (1997).
[64] E. Hille, *Analytic function theory II*, (Ginn and Co., Boston 1962).